Check for updates

View Article Online
View Journal

Journal of
Materials Chemistry C
Materials for optical, magnetic and electronic devices

Accepted Manuscript

This article can be cited before page numbers have been issued, to do this please use: S. Li, L. Xu, X. Kong, T. Kusunose, N. Tsurumachi and Q. Feng, *J. Mater. Chem. C*, 2020, DOI: 10.1039/C9TC05139B.

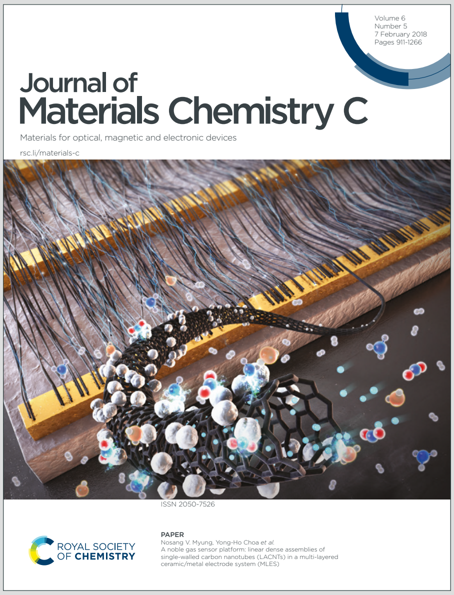

Volume 6
Number 5
7 February 2018
Pages 911-1266

Journal of
Materials Chemistry C
Materials for optical, magnetic and electronic devices
rsc.li/materials-c

ISSN 2050-7526

ROYAL SOCIETY OF CHEMISTRY

PAPER
Nosang V. Myung, Yong-Ho Choa *et al.*
A noble gas sensor platform: linear dense assemblies of single-walled carbon nanotubes (LACNTs) in a multi-layered ceramic/metal electrode system (MLES)

This is an Accepted Manuscript, which has been through the Royal Society of Chemistry peer review process and has been accepted for publication.

Accepted Manuscripts are published online shortly after acceptance, before technical editing, formatting and proof reading. Using this free service, authors can make their results available to the community, in citable form, before we publish the edited article. We will replace this Accepted Manuscript with the edited and formatted Advance Article as soon as it is available.

You can find more information about Accepted Manuscripts in the Information for Authors.

Please note that technical editing may introduce minor changes to the text and/or graphics, which may alter content. The journal's standard Terms & Conditions and the Ethical guidelines still apply. In no event shall the Royal Society of Chemistry be held responsible for any errors or omissions in this Accepted Manuscript or any consequences arising from the use of any information it contains.

ROYAL SOCIETY
OF CHEMISTRY

rsc.li/materials-c

View Article Online
DOI: 10.1039/C9TC05139B

Journal Name

ARTICLE

Published on 24 January 2020. Downloaded by Goteborgs Universitet on 1/28/2020 9:01:40 AM.

Received 00th January 20xx,
Accepted 00th January 20xx

DOI: 00.0000/x0xx00000x

Bismuth Chalcogenide Iodides of $Bi_{13}S_{18}I_2$ and BiSI: Solvothermal Synthesis, Photoelectric Behavior, and Photovoltaic Performance

Sen Li,[a] Linfeng Xu,[a] Xingang Kong,[b] Takafumi Kusunose,[a] Noriaki Tsurumach,[a] and Qi Feng [a]*

Bismuth chalcogenide iodides of $Bi_{13}S_{18}I_2$ and BiSI were synthesized and characterized as a light absorber for solar cells. The formations of $Bi_{13}S_{18}I_2$ and BiSI can be controlled via a facile solvothermal process. BiSI is formed under the lower S/Bi mole ratio conditions but it easily converts to $Bi_{13}S_{18}I_2$ under higher S/Bi mole ratio conditions. $Bi_{13}S_{18}I_2$ is an n-type semiconductor with a narrow bandgap of 0.75 eV and possesses a strong light absorbance in the wide wavelength range from UV to NIR, suggesting the promising light absorber material for solar cells. A uniform $B_{13}S_{18}I_2$ nanorods film was fabricated on a porous TiO_2 electrode via a modified solvothermal process for the photovoltaic study. The $Bi_{13}S_{18}I_2$-based solar cell demonstrates a power conversion efficiency of 0.85% for the first time, revealing the potential as a new type of light absorber material for solar cells which can be fabricated via a low-cost solution process.

Introduction

As the global demand for energy is expected to grow rapidly, the securing of clean energy is essential for sustainable economic growth. The solar energy is the most promising clean energy source for the next-generation.[1, 2] At present, the photovoltaic (PV) market is dominated by crystalline silicon panels which possess relatively high efficiency, but the high cost has prompted the development of low cost high performance PVs.[3] Some new types of PVs, such as the thin film type of $CuIn_{1-x}Ga_xSe_2$ (CIGS) and CdTe PVs, have been developed to reduce the cost and increase power conversion efficiency (PCE). Although the PCE of these PVs having recently reached 22%, their potential and future prospect are limited by the high cost of indium and scarcity of tellurium.[4, 5]

Recently the Pb-based hybrid halide perovskites, such as $CH_3NH_3PbI_3$ (MAPI), have attracted much attention as a promising solar light absorbers for PV due to the high PCE and the low cost of the solution fabrication process.[6, 7] Although it was first reported only 10 years ago, the PCE of the PVs using a hybrid perovskite as a light absorber has reached to 24.2%,[8] surpassing all other third-generation PVs, and this fast-growing PCE is a new record in the history of PV technology.[9] Unfortunately, in addition to humidity and thermal instability, the Pb-based hybrid halide perovskites pose a potential environmental risk due to leaching of toxic Pb.[10-12] In order to solve these problems, there is an urgent need to explore alternative light absorber materials consisting of nontoxic elements. The substitution of Pb(II) with Bi(III) in the hybrid perovskites is attractive because both Bi(III) and Pb(II) have the same $6s^26p^0$ electronic configuration, thus ensuring that their compounds will share similar properties. Some studies suggest that Bi-based hybrid perovskites are promising as the PV light absorber, but the success on the synthesis of Bi-based hybrid perovskites has not been reported.[13-16] A non-toxic bismuth-halide double perovskites $A_3Bi_2X_9$ (A = Cs^+, Ag, $CH_3NH_3^+$ and $HC(NH_2)^{2+}$; X = I^-, Br^-, Cl^-) have been much investigated and employed for solar cells,[16] just possessing a PCE of 3.2% up to now.[17]

Recently, some V-VI-VII compounds (V=Sb, Bi, VI=O, S, Se, VII= Cl, Br, I), have attracted much attention as potential electronic materials. These compounds exhibit a variety of physical characteristics, including high photoconductivity, ferroelectric photovoltaic effect,[18] piezoelectricity, electrooptical effect,[19, 20] and structural diversity.[13, 14] BiSX compounds have attracted significant attention as PV materials because of their excellent semiconducting properties and narrow bandgaps, which can absorb the solar spectrum in a wide wavelength range.[21, 22] Another important advantage is that the bandgaps are tunable via substitution between halogens each other, such as $BiSBr_{1-x}I_x$ solid solutions.[23] Recently, Hahn et al. have described a solar cell using a BiSI semiconductor thin film as a lighter-absorber, which yielded a PCE of 0.25%.[24] Tiwari et al. described a BiSI-based solar cell with a record PCE of 1.32% by employing p-type organic semiconductor as hole transport material.[25] BiOX compounds possess tunable bandgaps from 3.46 eV for BiOCl to 1.77 eV for BiOI, and exhibit superior photocatalytic activities.[21, 26] BiSX compounds are synthesized generally using a vapor

---

[a] Department of Advanced Materials Science, Faculty of Engineering and design, Kagawa University, 2217-20 Hayashi-cho, Takamatsu 761-0396, Japan
[b] School of Materials Science and Engineering, Shaanxi University of Science and Technology, Weiyang, Xi'an, Shaanxi, 710021 PR China

Electronic Supplementary Information (ESI) available: Bismuth Chalcogenide Iodides of $Bi_{13}S_{18}I_2$ and BiSI: Solvothermal Synthesis, Photoelectric Behavior, and Photovoltaic Performance. See DOI: 000.0000/x0xx00000x

Journal of Materials Chemistry C Accepted Manuscript

This journal is © The Royal Society of Chemistry 20xx

View Article Online
DOI: 10.1039/C9TC05353H

Published on 24 January 2020. Downloaded by Goteborgs Universitet on 1/28/2020 9:01:40 AM.

Journal of Materials Chemistry C Accepted Manuscript

transport process at high temperature above 400 °C in a vacuum tube.[27] BiSI can also be obtained through a solvothermal process and melt growth process by the Bridgeman-Stockbarger technique.[20, 28]

Fewer studies have been reported on $Bi_{19}S_{27}X_3$ (X=Cl, Br, I) compounds. Traditionally, these bismuth sulfohalogenides are synthesized using a vapor transport process and flux process under high temperature conditions over 600°C.[29, 30] A solvothermal process has also been employed to obtain $Bi_{19}S_{27}X_3$ nanocrystals.[31-33] The $Bi_{19}S_{27}Br_3$ and $Bi_{19}S_{27}Cl_3$ nanocrystals exhibit efficient photocatalytic degradation of 2,4-dichorophenol and the reduction of Cr(VI).[32, 33] The characteristics and structure of $Bi_{19}S_{27}I_3$ remain unclear. Ho et al. have reported that this compound possesses an indirect bandgap at 0.73 eV and a direct bandgap at 1.08 eV, respectively.[30] However, Groom et al. have reported that this compound is an indirect bandgap semiconductor based on the single crystal structure study and electronic structure calculations, furthermore, the result also revealed that this compound can be expressed as a new composition formula of $Bi_{13}S_{18}I_2$.[29] Very recently, Yan et al. have fabricated the $Bi_{19}S_{27}I_3$ nanorod cluster films through a solvothermal process and applied the film to a photodetector.[34] However, to the best of our knowledge, the $Bi_{13}S_{18}I_2$-based solar cells have not been reported yet.

Herein, we report a facile solvothermal process for the synthesis of bismuth chalcogenide iodides of $Bi_{13}S_{18}I_2$ and BiSI and systematical characterization of their photoelectric behavior as a light absorber for solar cells. A possible formation mechanism for $Bi_{13}S_{18}I_2$ and BiSI under the solvothermal conditions is proposed. Both $Bi_{13}S_{18}I_2$ and BiSI are n-type semiconductors with the bandgaps of 0.75 and 1.57 eV, respectively. We modified the solvothermal process to fabricate $Bi_{13}S_{18}I_2$ nanorod film on a porous TiO_2 nanocrystal film for a new type of $Bi_{13}S_{18}I_2$-based solar cells. The preliminary PV study gave a PCE of 0.85%, suggesting the potential of the $Bi_{13}S_{18}I_2$-based solar cells which can be fabricated by the low-cost solution process.

Experimental details

Chemicals and reagents.

Hydroiodic acid (HI, 57% in water), and BiI_3 (98%) were purchased from Sigma-Aldrich. CH_4N_2S (99.0%) from TCI chemistry and ethylene glycol, acetone and dimethyl sulfoxide (DMSO) were bought from Wako Chemicals. All chemicals and reagents were analytical grade and used as received.

Synthesis of bismuth chalcogenide iodide powder samples.

CH_3NH_3I (MAI) was synthesized by the reaction of 24 mL of methylamine and 10 mL of HI solution at 0 °C for 2 h in a rotary evaporator at 120 rpm, and then evaporated at 80 °C. The precipitate was washed three times with ethanol and then diethyl at room temperature and then dried at 60 °C for 24 h. For the synthesis of a bismuth chalcogenide iodide powder sample, BiI_3 (2 mmol), MAI (3 mmol), and a desired amount of CH_4N_2S were added into 5 mL of ethylene glycol solvent. The mixture was solvothermally treated at a desired temperature for 12 h under stirring conditions. The obtained sample was filtrated, washed with ethanol, and then dried in a drying oven at 60 ^oC for 12 h.

Fabrication of bismuth chalcogenide iodide pellet samples.

Synthesized bismuth chalcogenide iodide powder sample was gently ground into fine powder. This powder sample was then pressed using a pallet press mold with a diameter of 10 mm at 30 MPa for 3 min. Subsequently, cold isostatic press (CIP) treatment was employed on the pellet sample with a pressure of 200 MPa for 5 min to increase sample density. The thickness of the pellet was about 1 mm.

Fabrication of TiO_2 Electrode.

A TiO_2 nanocrystal paste was prepared by mixing a P25 TiO_2 nanocrystal sample (0.5 g), ethanol (2.5 g), α-terpineol (2.0 g), a 10 wt % solution of ethyl-cellulose 10 (1.4 g), and a 10 wt % solution of ethyl-cellulose 45 (1.1 g). The mixture was dispersed by ultrasonication for 30 min and then ball-milling for 72 h. After ball-milling, the ethanol was removed from the mixture using a rotary evaporator.[35]

The TiO_2 electrode was prepared in the following manner.[36] The fluorine-doped tin oxide (FTO) conducting glass plate was cleaned in distilled water and acetone by ultrasonication for 10 min, consecutively. Then the FTO glass plate was dipped in 0.1 M titanium tetraisopropoxide (TTIP) solution for 1 min and washed with distilled water and ethanol, dried at room temperature, and calcined at 480 °C for 1 h to coat the FTO glass surface with a dense TiO_2 thin film. The prepared TiO_2 paste was then coated on the dense TiO_2 thin film on the FTO glass plate by a screen printing technique and dried at 120 °C for 10 min. This process was repeated to obtain TiO_2 nanocrystal film of about 10 μm in thickness. After the TiO_2 paste coating, the TiO_2 film was calcined at 450 °C for 30 min to obtain a TiO_2 nanoporous electrode. The TiO_2 nanoporous electrode was dipped in the 0.1 M TTIP solution for 1 min, washed with distilled water and ethanol, dried at room temperature, and calcined at 480 °C for 1 h again.

Fabrication of $Bi_{13}S_{18}I_2$ film on TiO_2 Electrode.

0.4 mmol BiI_3 (0.2359 g), 0.6 mmol MAI (0.0954 g), and 1.6 mmol CH_4N_2S (1.2179 g) were dissolved in 1 mL ethylene glycol solvent by stirring for 1 h, and then a red BiI_3-MAI-CH_4N_2S mixed solution was obtained. The mixed solution was coated on the TiO_2 nanoporous electrode surface. After standing for 2 h, the coated TiO_2 nanoporous electrode was placed on a shelf set in a Teflon-lined stainless steel autoclave with an internal volume of 80 mL. After adding 1 mL ethylene glycol solvent to the autoclave bottom, the autoclave was sealed and solvothermally treated at 195 ^oC for 12 h. After cooling to room temperature, a black $Bi_{13}S_{18}I_2$-coated TiO_2 electrode was obtained. The $Bi_{13}S_{18}I_2$-coated TiO_2 electrode was washed with ethanol and then dried at 60 ^oC for 12 h in a drying oven.

Fabrication and characterization of solar cells.

The $Bi_{13}S_{18}I_2$-solar cell was comprised of the $Bi_{13}S_{18}I_2$-coated TiO_2 electrode as an anode, Pt-coated FTO glass as a cathode, and an electrolyte solution between the anode and the cathode. The electrolyte solution contained 0.1 M LiI, 0.01 M I_2, 0.6 M 1-butyl-3-n-propylimidazolium iodide (BMII), 0.4 M 4-tert-butylpyridine (TBP), and 0.1 M guanidine thiocyanate (GT) in a mixed solvent of acetonitrile and valeronitrile (v/v = 85:15). The photocurrent−voltage characteristic curve for the $Bi_{13}S_{18}I_2$-solar cell was measured using a Hokuto-Denko BAS100B electrochemical analyzer under irradiation with simulated sunlight of AM 1.5 (100 mW/cm^2), using a sunlight simulator (YSS-E40, Yamashita Denso). A light-passing mask was fixed on the surface of the FTO glass of

View Article Online
DOI: 10.1039/C9TC05139B

Published on 24 January 2020. Downloaded by Goteborgs Universitet on 1/28/2020 9:01:40 AM.

Journal of Materials Chemistry C Accepted Manuscript

the anode to set the effectively irradiating area on the cell at 0.25 cm^2.

Physical analysis.

The crystal structures of the samples were investigated using a powder X-ray diffractometer (Shimadzu, model XRD-6100) with Cu Kα (λ= 0.1542 nm) radiation. The morphology of the samples was observed using field emission scanning electron microscopy (FE-SEM) (JEOL, ISM-7001F) and the chemical composition was measured using energy dispersive X-ray spectroscopy (EDX) attached to the FE-SEM at 15 kV of acceleration voltage. Transmission electron microscopy (TEM) and high-resolution TEM (HR-TEM) observations were performed on a JEOL Model JEM-3010 system at 300 kV. The Mott-Schottky plot was measured using an electrochemical analyzer (Shanghai Chenhua, CHI660E). The ultraviolet-visible-near infrared (UV-Vis-NIR) absorption spectrum was obtained on a Shimadzu solidspec-3700 UV-Vis-NIR spectrophotometer at room temperature. The TG-DTA analysis was carried out using a thermal analyzer (Shimadzu, DTG-60H) at a heating rate of 10 °C/min. For the conductivity measurement, a voltage of 100 V was applied to the pellet sample, and the current was measured using a ferroelectric testing system (Toyo Corporation, FCE3-4KVSYS) at room temperature. X-ray photoelectron spectroscopy (XPS) was performed using a Kratos AXIS SUPRA X-ray photo-electron spectrometer. The XPS spectra were calibrated to the adventitious carbon peak at 284.8 eV.

Results and discussion

Solvothermal synthesis of bismuth chalcogenide iodide compounds.

The bismuth chalcogenide iodide compounds of $Bi_{13}S_{18}I_2$ and BiSI were synthesized by solvothermal treatment of a mixture of BiI_3, CH_4N_2S, and CH_3NH_3I (MAI) in an ethylene glycol solvent. The formation of the bismuth chalcogenide iodide compounds is strongly dependent on the CH_4N_2S/BiI_3/MAI mole ratio and reaction temperature. Fig. 1 shows the XRD patterns of the samples synthesized under the conditions of different CH_4N_2S/BiI_3 mole ratios at 195 °C, where the BiI_3/MAI mole ratio was fixed at 2:3. In this reaction system, the iodine amount was excessive for the formation of $Bi_{13}S_{18}I_2$ and BiSI because the mole ratios of Bi/S/I are 13:18:2 in $Bi_{13}S_{18}I_2$ and 1:1:1 in BiSI, respectively. The XRD pattern of the sample prepared at a CH_4N_2S/BiI_3 mole ratio of 1:2 can be well indexed to an orthorhombic BiSI phase with a space group of *Pnma* and lattice constants of a = 0.8519, b = 1.0177 and c = 0.4172 nm (JCPDS File No.73-1171). By increasing CH_4N_2S/BiI_3 mole ratio, the $Bi_{13}S_{18}I_2$ phase (JCPDS File No. 73-1157) was formed and became main phase with small amount of metal Bi phase at CH_4N_2S/BiI_3 = 3:2, and then the single $Bi_{13}S_{18}I_2$ phase was formed at CH_4N_2S/BiI_3 = 4:2. The structure of the $Bi_{13}S_{18}I_2$ phase belongs to a hexagonal system with a space group of $P6_3$ and lattice parameters of a = 1.5612 and c = 0.4017 nm.[29] When the CH_4N_2S/BiI_3 mole ratio was increased to 8:2, the $Bi_{13}S_{18}I_2$ phase disappeared, where a Bi_2S_3 single phase was formed. The above results reveal that the products are sensitive to the Bi/S mole ratio in this solvothermal reaction system.

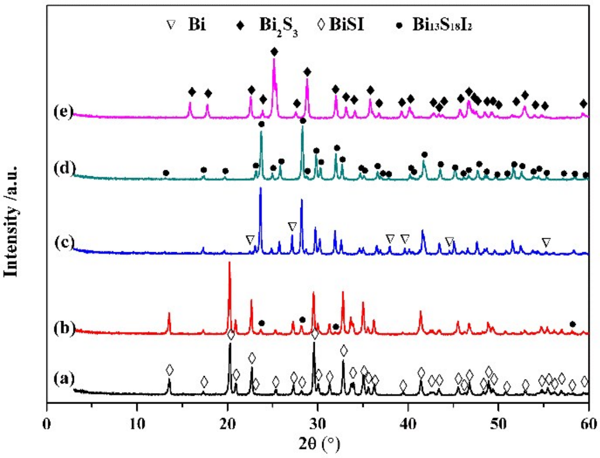

Fig. 1. XRD patterns of products obtained by solvothermal treatments of solutions with CH_4N_2S/BiI_3/MAI mole ratios of (a) 1:2:3, (b) 2:2:3, (c) 3:2:3, (d) 4:2:3, and (e) 8:2:3 at 195 °C for 12h, respectively.

To provide a phase diagram for the BiI_3-CH_4N_2S-MAI solvothermal reaction system, the solvothermal treatments were carried out at different temperatures and the XRD patterns of the products are shown in Fig. S1. Based on the XRD results, the phase diagram for the BiI_3-CH_4N_2S-MAI solvothermal reaction system was obtained as shown in Fig. 2. BiSI is preferably formed in low S/Bi mole ratio range below 1.5, namely the Area-A. By increasing the S/Bi mole ratio, a mixture of the BiSI, $Bi_{13}S_{18}I_2$, small amount of metal Bi, and an unknown phase is formed in Area-B. The single $Bi_{13}S_{18}I_2$ phase can be obtained in Area-C. By further increasing the S/Bi mole ratio, Bi_2S_3 is formed in Area-D, and the Bi_2S_3 single phase is formed in Area-E, suggesting that $Bi_{13}S_{18}I_2$ is unstable under the high S/Bi mole ratio conditions in the BiI_3-CH_4N_2S-MAI solvothermal reaction system.

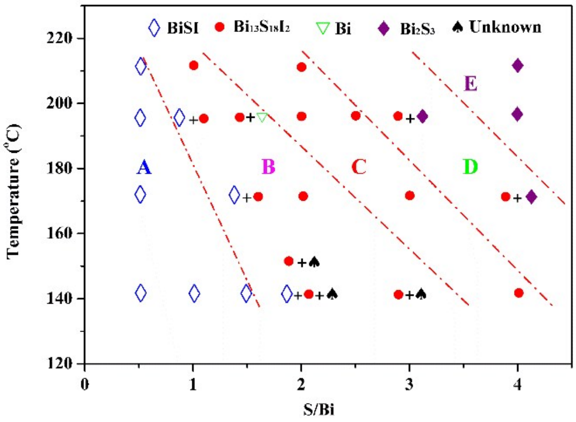

Fig. 2. Phase diagram for BiI_3-CH_4N_2S-MAI solvothermal reaction system in ethylene glycol solution with mole ratio of BiI_3/MAI = 2:3. Area-A: BiSI; Area-B: mixture of BiSI, $Bi_{13}S_{18}I_2$, Bi and unknown phase; Area-C: $Bi_{13}S_{18}I_2$; Area-D: mixture of $Bi_{13}S_{18}I_2$ and Bi_2S_3; Area-E: Bi_2S_3.

View Article Online
DOI: 10.1039/C9TC05139B

Published on 24 January 2020. Downloaded by Goteborgs Universitet on 1/28/2020 9:01:40 AM.

We also tried to synthesize bismuth chalcogenide iodide compounds in other solvents, such as acetone, DMF, and DMSO. The XRD patterns of the solvothermal products prepared at $CH_4N_2S/BiI_3/MAI = 4:2:3$ (S/Bi = 2:1) mole ratio and 195 °C are shown in Fig. S2. Although the single phase of $Bi_{13}S_{18}I_2$ can be formed in acetone solvent, the yield of $Bi_{13}S_{18}I_2$ is disappointing, due to the low reactivity in this solvent. In the DMF solvent, a mixture of the $Bi_{13}S_{18}I_2$ phase and metal Bi phase is formed. However, an unknown phase without $Bi_{13}S_{18}I_2$ is formed in the DMSO solvent. These results suggest that the solvothermal formations of bismuth chalcogenide iodine compounds are sensitive to the solvents. Compared with the high temperature reaction process,[29, 30] the solvothermal process described above is a facile method for the synthesis of the bismuth chalcogenide iodide compounds.

FE-SEM was employed to investigate the morphology of products obtained by the solvothermal reaction and the results for the samples prepared at 195 °C are shown in Fig. 3 The sample obtained at a mole ratio of $CH_4N_2S/BiI_3 = 1:2$ possesses a fibrous particle morphology with a diameter of about 500 nm and a length of about 20 μm (Fig. 3(a)). The fibrous particles correspond to BiSI because this sample is a BiSI single phase (Fig. 1(a)). The fibrous particles and urchin-like particles were observed in the sample of mixed BiSI and $Bi_{13}S_{18}I_2$ phases obtained at a mole ratio of $CH_4N_2S/BiI_3 = 2:2$ (Fig. 3(b)), where the fibrous particles can be attributed to the BiSI phase and the urchin-like particles to the $Bi_{13}S_{18}I_2$ phase (Fig. 1(b)). The $Bi_{13}S_{18}I_2$ single phase sample obtained at a mole ratio of $CH_4N_2S/BiI_3 = 4:2$ exhibits a rod-like particle morphology with a diameter of about 400 nm and a length of about 5 μm (Fig. 3(c)). The Bi_2S_3 single phase sample obtained at a mole ratio of $CH_4N_2S/BiI_3 = 8:2$ shows fibrous and rod-like particle morphologies (Fig. 3(d)).

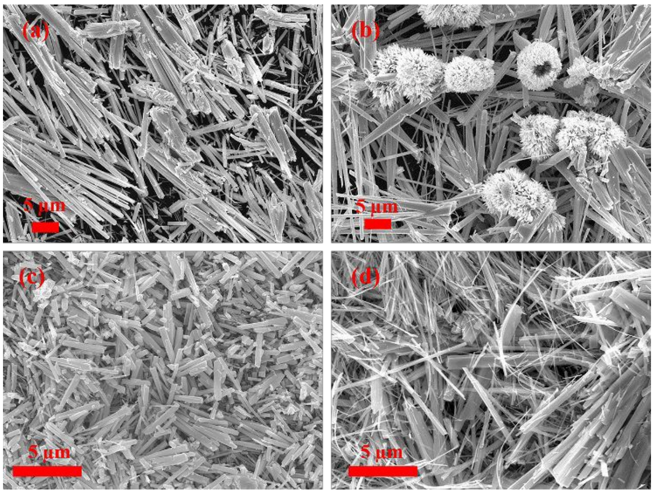

Fig. 3. FE-SEM images of products synthesized by solvothermal treatments of solutions with $CH_4N_2S/BiI_3/MAI$ mole ratios of (a) 1:2:3, (b) 2:2:3, (c) 4:2:3, (d) 8:2:3 at 195 °C for 12 h, respectively.

The $Bi_{13}S_{18}I_2$ possesses an interesting structure, as shown in Fig. 4(a).[27] In this structure, ribbon-like subunits of $[Bi_4S_6]$ form six spokes around a central hexagonal channel at the corners of the unite cell. The $[Bi_4S_6]$-ribbons spokes are connected together to form a triangular tunnel structure in the direction of c-axial, where I^- located in the tunnel site of the $Bi_{13}S_{18}I_2$ structure. TEM and HRTEM results revealed that the rod-like $Bi_{13}S_{18}I_2$ particles were single crystals, where the rod-like crystal axis direction corresponds to [001] (Fig. S3); in other words, $Bi_{13}S_{18}I_2$ crystals grow in the direction c-axial. Zhou et al. have proposed that such ribbon structural geometry can exhibit a high conductivity along covalently bonded $[Bi_4S_6]$-ribbons direction, i.e, the direction of the c-axis, which gives several advantages as light absorbers for solar cells.[37]

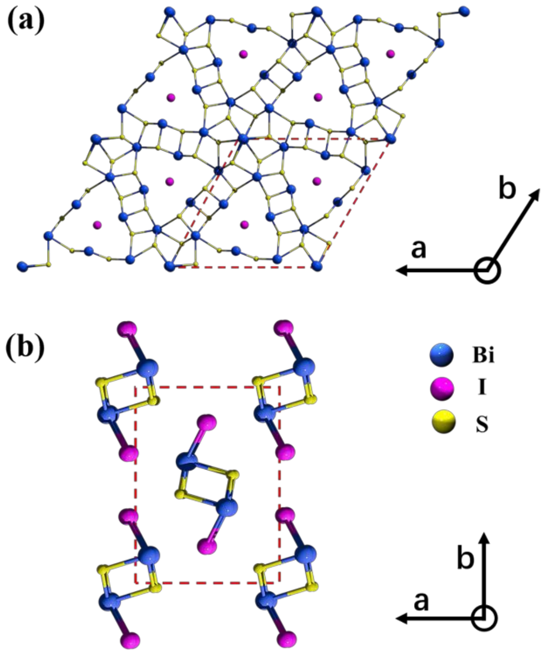

Fig. 4. Structures of (a) hexagonal $Bi_{13}S_{18}I_2$ and (b) orthorhombic BiSI.

In the BiSI structure, double chain subunit of $[(BiSI)_2]$ is formed by linking Bi with S and I together by strong Bi-S and Bi-I bonds along the direction of c-axis, and the $[(BiSI)_2]$-chains are held together by weak Van der Waals type bonds, as shown in Fig. 4 (b).[38] TEM and HRTEM results reveal that rod-like BiSI particles were also single crystals and the rod-like crystals grew along the direction of c-axial in the similar manner as the $Bi_{13}S_{18}I_2$ structure (Fig. S3).

Formation reactions of bismuth chalcogenide iodide compounds

The BiI_3-CH_4N_2S-MAI mixed solution with a mole ratio of 2:4:3 $CH_4N_2S/BiI_3/MAI$ was solvothermally treated at 195 °C for different reaction times to investigate the formation process of bismuth chalcogenide iodide compounds. XRD results indicate that a binary mixture of BiSI and $Bi_{13}S_{18}I_2$ was formed after the reaction for 0.5 h (Fig. 5). By prolonging the reaction time, the fraction of BiSI decreased and that of $Bi_{13}S_{18}I_2$ increased, then the BiSI disappeared completely after 6 h reaction, and finally the $Bi_{13}S_{18}I_2$ single phase was formed after 12 h reaction. This result suggests that first BiSI is formed, which then converts to $Bi_{13}S_{18}I_2$ under the solvothermal reaction conditions.

Journal of Materials Chemistry C Accepted Manuscript

View Article Online
DOI: 10.1039/C9TC05139B

Published on 24 January 2020. Downloaded by Goteborgs Universitet on 1/28/2020 9:01:40 AM.

Journal of Materials Chemistry C Accepted Manuscript

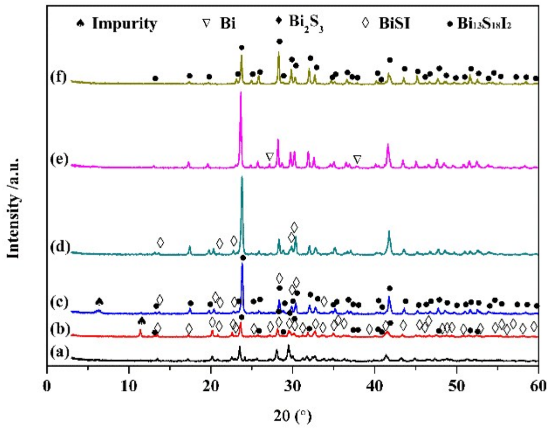

Fig. 5. XRD patterns of products synthesized by solvothermal treatments of solution with CH_4N_2S/BiI_3/MAI mole ratios of 4:2:3 at 195 °C for (a) 0.5, (b) 1, (c) 2, (d) 4, (e) 6, (f) 12 h, respectively.

The conversion reaction of BiSI to $Bi_{13}S_{18}I_2$ was investigated by FE-SEM observation (Fig. 6(A)). In the sample obtained after 0.5 h reaction, large fibrous particles and small urchin-like particles were observed simultaneously. Energy dispersive X-Ray spectroscopy (EDS) analysis reveals that the large fibrous particles and small urchin-like particles have element compositions close to the stoichiometric compositions of BiSI (Bi/S/I =1:1:1) and $Bi_{13}S_{18}I_2$ (Bi/S/I =13:18:2), respectively (Figure S4 and Table S1); that is to say, they correspond to the BiSI phase and $Bi_{13}S_{18}I_2$ phase, respectively. By increasing the reaction time up to 4 h, the urchin-like $Bi_{13}S_{18}I_2$ particles grew up and their fraction in the product increased, accompanying the consumption of the fibrous BiSI particles. After 6 h reaction, the urchin-like $Bi_{13}S_{18}I_2$ particles became to rod-like in shape and the fibrous BiSI particles disappeared completely. This reaction process can be confirmed by element composition analysis results of SEM-EDS in Fig. S4 and Table S1, and also corresponds to the XRD results in Fig. 5.

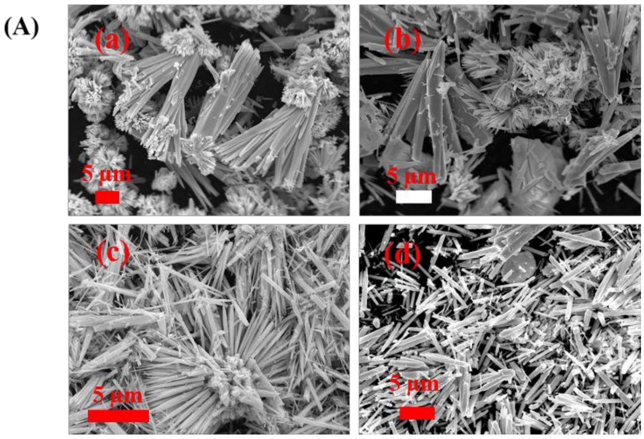

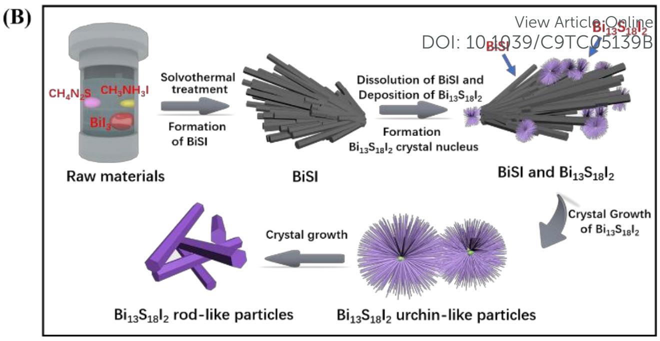

Fig. 6. (A). FE-SEM images of products synthesized by solvothermal treatments of solution with CH_4N_2S/BiI_3 /MAI mole ratios of 4:2:3 at 195 °C for (a) 0.5, (b) 1, (c) 2, (e) 6 h respectively. (B). Schematic illustration of formation reaction mechanism of BiSI and $Bi_{13}S_{18}I_2$.

Based on the results described above, we deduced a reaction mechanism for the formation of BiSI and $Bi_{13}S_{18}I_2$ in the solvothermal reaction system, as shown in Fig. 6(B). In the first step, S^{2-} is formed by the decomposition reaction of CH_4N_2S under solvothermal conditions and then BiSI is formed by the solution reaction of Bi(III), S^{2-} and I^-, resulting in the fibrous BiSI particles. In the second step, the crystal nuclei of $Bi_{13}S_{18}I_2$ are formed on surface of the fibrous BiSI particles (Fig. 6 (A)(a)) and then they grow up to the small urchin-like $Bi_{13}S_{18}I_2$ particles through a BiSI-dissolution reaction and a $Bi_{13}S_{18}I_2$-deposition reaction. In the third step, the small urchin-like $Bi_{13}S_{18}I_2$ particles further grow up and finally collapse, becoming the individual rod-like $Bi_{13}S_{18}I_2$ particles through the BiSI-dissolution reaction and the $Bi_{13}S_{18}I_2$-deposition reaction. Thus, the BiSI phase is converted to the $Bi_{13}S_{18}I_2$ phase in this reaction system.

Characterization of bismuth chalcogenide iodide compounds

It has been reported that BiSI can be used as a light absorber for solar cells.[4] In the present study, therefore, we investigated the thermostabilities and photoelectric properties of $Bi_{13}S_{18}I_2$ and BiSI to evaluate the potential of $Bi_{13}S_{18}I_2$ as a light absorber for a new type of solar cells. The $Bi_{13}S_{18}I_2$ and BiSI samples synthesized by solvothermal treatment of the CH_4N_2S-BiI_3-MAI mixed solution with CH_4N_2S/BiI_3/MAI mole ratios of 4:2:3 and 1:2:3 at 195 °C for 12 h, respectively, were used for the characterization. The TG-DTA analysis and XRD results (Fig. S5 and S6) suggest that $Bi_{13}S_{18}I_2$ is stable up to 350 °C, decomposes to BiOI at around 380 °C and finally to Bi_2O_3 at above 500 °C. Similar to $Bi_{13}S_{18}I_2$, BiSI is stable up to 400 °C, decomposes to BiOI at around 400 °C and finally to Bi_2O_3 at above 500 °C (Fig. S5 and S6). BiSI exhibits a slightly higher thermostability than $Bi_{13}S_{18}I_2$ in air.

The pellet samples of $Bi_{13}S_{18}I_2$ and BiSI were used for the conductivity measurement at room temperature (Fig. S7). The electrical conductivity (σ) was calculated from the applied voltage (V), measured current (I), thickness of pellet (L), and area (S) of the pellet sample using formula (1).

$$\boldsymbol{\sigma} = \frac{\boldsymbol{I * L}}{\boldsymbol{V * S}} \qquad (1)$$

The calculated electrical conductivity of the $Bi_{13}S_{18}I_2$ pellet sample is 8.85×10^{-7} S/cm, which is much lower than the

Please do not adjust margins

View Article Online
DOI: 10.1039/C9TC06551H

Published on 24 January 2020. Downloaded by Goteborgs Universitet on 1/28/2020 9:01:40 AM.

Journal of Materials Chemistry C Accepted Manuscript

reported value of 9×10^{-4} S/cm for a single crystal sample.[30] The lower conductivity of the $Bi_{13}S_{18}I_2$ pellet sample can be attributed to the low density of the pellet sample and the grain boundaries because of the rod-like particle morphology of $Bi_{13}S_{18}I_2$, which can be confirmed in its FE-SEM image (Fig. S8). The BiSI pellet sample has an electrical conductivity of 6.24×10^{-7} S/cm.

The $Bi_{13}S_{18}I_2$ and BiSI samples are black crystals. The UV-Vis-NIR absorption spectra of $Bi_{13}S_{18}I_2$ and BiSI are shown in Fig. 7A. A strong and broad absorption peak around 500 nm in the visible light wavelength range and another strong peak at 1115 nm in the near-IR wavelength range were observed in the $Bi_{13}S_{18}I_2$ absorption spectrum. A strong flat absorbance in the wavelength range of 300 to 800 nm was observed in the BiSI absorption spectrum. The absorption spectra findings reveal that $Bi_{13}S_{18}I_2$ has a smaller bandgap energy than that of BiSI and is a promising light absorber for solar cells.

The bandgap energy (E_g) of a semiconductor can be estimated using Tauc's formula $(Ah\nu)^{1/n} = B(h\nu-E_g)$, where A, B, and $h\nu$ are the absorption coefficient, a constant, and the incident photon energy, and the exponent n is equal to 1/2 or 2 for the allowed direct or indirect transition, respectively.[39] Because $Bi_{13}S_{18}I_2$ and BiSI are indirect semiconductors,[29, 38, 40] Taus's formula can be represented as the Kubelka–Munk function $A = C(h\nu-E_g)^2/h\nu$, where C is the absorption constant.[19, 41] The bandgap energy can be estimated from the transformed Kubelka–Munk function versus the photon energy (Fig. 7(b) and (d)). The estimated bandgap energy of the $Bi_{13}S_{18}I_2$ sample was 0.75 eV by extrapolating the straight line to zero absorption intercepting the ($h\nu$) axis. It would be noticed the absorption does not fall to zero at 0.75 eV, which suggests that the true bandgap may be lower than 0.75 eV as Groom et al. reported.[29] The bandgap value corresponds that reported by Ho et al's.[30] Yan et al. reported a direct band gap of 0.83 eV that is slightly larger than our result.[34] The BiSI sample has a bandgap energy of 1.57 eV, which agrees with reported values of 1.57-1.59 eV.[4, 22, 40]

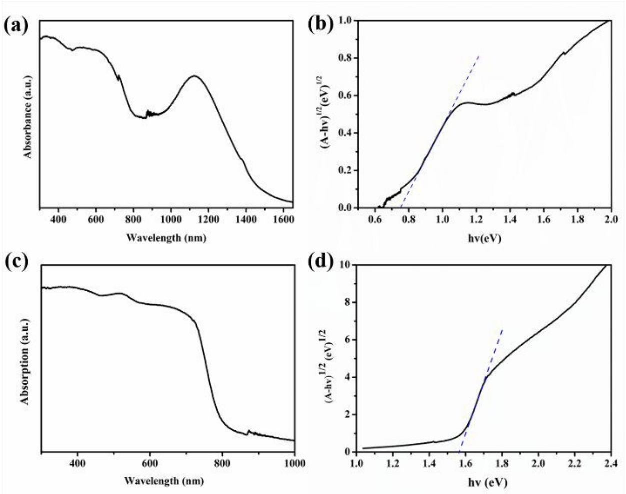

Fig. 7. UV-Vis-NIR absorption spectra and corresponding plots of transformed Kubelka-Munk function versus *hν* for (a, b) $Bi_{13}S_{18}I_2$ and (c, d) BiSI powder samples, respectively.

X-ray photoelectron spectroscopy (XPS) was used to investigate the surface valence state and the chemical composition of the $Bi_{13}S_{18}I_2$ and BiSI samples. The XPS survey spectrum reveals the predominant presence of sulfur, bismuth and iodine, as well as a small amount of carbon and oxygen impurities in both $Bi_{13}S_{18}I_2$ and BiSI samples (Fig. S9). The carbon and oxygen may correspond to the residual orgonic precursor and adsorbed oxygen molecules on the particle surface. The Bi spin-orbit doublet peaks of BiSI is consistent with the XPS result of BiSI reported by Grigas et al., where all Bi are trivalent in BiSI.[42] The Bi-4f$_{7/2}$ and Bi 4f$_{5/2}$ peaks were observed at 158.7 and 164.0 eV for BiSI and at 158.0 and 163.3 eV for $Bi_{13}S_{18}I_2$. The different binding energies between $Bi_{13}S_{18}I_2$ and BiSI may account for the existence of bivalent Bi(II) in $Bi_{13}S_{18}I_2$. It has been reported that the bivalent Bi(II) as Bi_2^{4+} dimers is possible in $Bi_{13}S_{18}I_2$, which results in the formation of $(Bi^{3+})_{12}(Bi_2^{4+})_{0.5}(S^{2-})_{18}(I^-)_2$ rather than $Bi_{19}S_{27}I_3$ or $(Bi(Bi_2S_3)_9I_3)_{2/3}$.[29] The XPS result indicates that the atomic ratio of I/Bi/S in the $Bi_{13}S_{18}I_2$ sample is 1:6.5:8.9, which is very close to the stoichiometric mole ratio of 1:6.5:9.0 of $(Bi^{3+})_{12}(Bi_2^{4+})_{0.5}(S^{2-})_{18}(I^-)_2$. A single peak of S-2s was observed at 225.0 and 225.2 eV for $Bi_{13}S_{18}I_2$ and BiSI, respectively. The I-3d$_{3/2}$ and I-3d$_{5/2}$ spin-orbit spin components were observed at 630.1 and 618.6 eV for $Bi_{13}S_{18}I_2$ and 630.2 and 618.7 eV for BiSI, respectively. The binding energies of S-2s, I-3d$_{3/2}$ and I-3d$_{5/2}$ of $Bi_{13}S_{18}I_2$ are very close to those of BiSI.

Fig. 8 shows the valance-band spectra of $Bi_{13}S_{18}I_2$ and BiSI. The valence band maximum is located at 0.61 and 0.89 eV below the Fermi level for $Bi_{13}S_{18}I_2$ and BiSI, respectively. Therefore, the conduction band minimum of $Bi_{13}S_{18}I_2$ will be located at 0.14 eV above the Fermi level because the band gap of $Bi_{13}S_{18}I_2$ is 0.75 eV. As the Femi level is close to the conduction band minimum, $Bi_{13}S_{18}I_2$ should be an n-type semiconductor.[43] This is different from the result that $Bi_{13}S_{18}I_2$ is a p-type semiconductor based on a Hot-probe measurement result.[30] The n-type and p-type semiconductors can be distinguished also by Mott-Schottky plot, where n-type semiconductor shows positive slope value and p-type semiconductor shows a negative slope value.[45] The Mott-Schottky plot of $Bi_{13}S_{18}I_2$ shows a positive slope value, as shown in Fig. S10, namely it is an n-type semiconductor.

There is also an argument about $Bi_{13}S_{18}I_2$ is an indirect bandgap semiconductor or a direct bandgap semiconductor.[29, 30] These arguments suggest that the properties of $Bi_{13}S_{18}I_2$ are strongly dependent on its synthesis conditions, maybe slightly different in the chemical composites, due to formation of the bivalent $[Bi_2]^{4+}$ dimer. Therefore, $Bi_{13}S_{18}I_2$ may be a tunable semiconducting material. On the other hand, the conduction band minimum of BiSI will be located at 0.68 eV above the fermi level because its bandgap energy is 1.57 eV. Therefore, BiSI should be also an n-type semiconductor because the Femi level was close to the conduction band minimum, which is agreement with the results reported.[4]

Please do not adjust margins

View Article Online
DOI: 10.1039/C9TC05139B

Published on 24 January 2020. Downloaded by Goteborgs Universitet on 1/28/2020 9:01:40 AM.

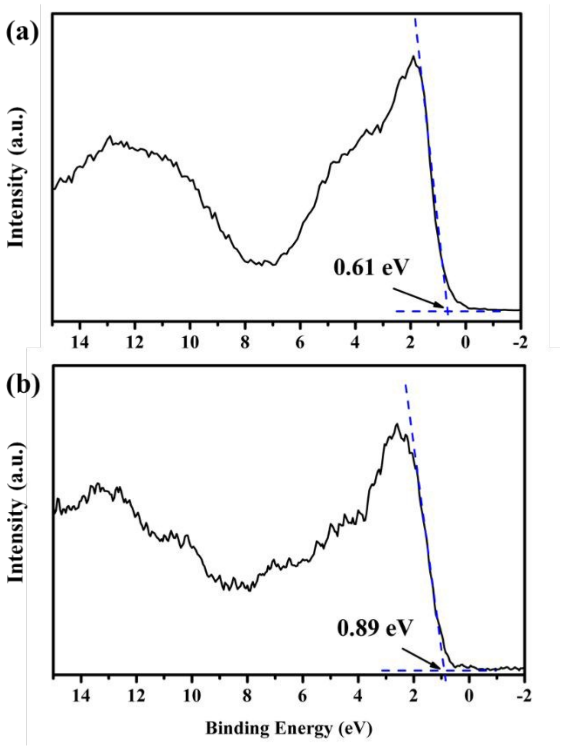

Fig. 8. Valance-band XPS spectra of (a) $Bi_{13}S_{18}I_2$ and (b) BiSI.

Solar cell performance of $Bi_{13}S_{18}I_2$ as light absorber

$Bi_{13}S_{18}I_2$ holds promise as a light absorber for solar cells because it exhibits strong light absorption in the whole visible light wavelength range as shown in Fig. 8(a). However, to the best of our knowledge, no any study has been reported on the application of $Bi_{13}S_{18}I_2$ as a light absorber for solar cells. Therefore, we carried out a preliminary PV study using $Bi_{13}S_{18}I_2$ as a light absorber to confirm its possibility. First, $Bi_{13}S_{18}I_2$ solar cells with a cell structure as shown in Fig. 9(a) were fabricated. In the solar cell, a TiO_2 dense film was coated on the surface of FTO conducting glass as a hole blocking layer and a TiO_2 porous film was coated on the TiO_2 dense film. A $Bi_{13}S_{18}I_2$ film was fabricated on the TiO_2 porous film using a modified solvothermal process. An electrolyte solution of I_3^-/I^- redox couple was used as the hole-transporting material and a Pt-coated FTO conducting glass was used as a counter-electrode similar to the dye-sensitized solar cells (DSSCs).

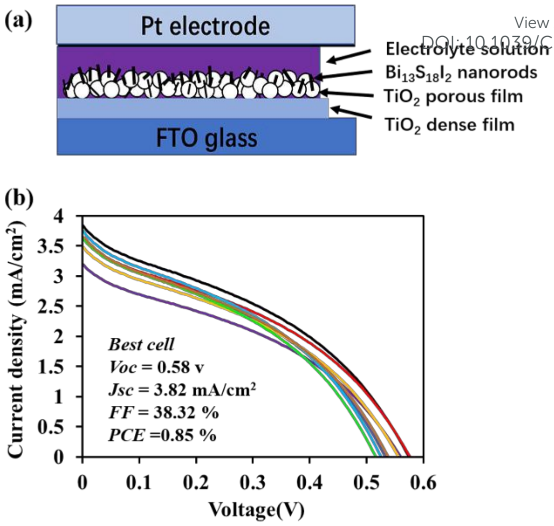

Fig. 9. (a) Schematic illustration of $Bi_{13}S_{18}I_2$-based solar cell structure and (b) *I-V* curves of eight $Bi_{13}S_{18}I_2$-based solar cells.

The FE-SEM images of $FTO/TiO_2/Bi_{13}S_{18}I_2$ electrode reveal that the thickness of the porous TiO_2 film was about 10 µm (Fig. 10(a)). A uniform black $Bi_{13}S_{18}I_2$ film was formed on the porous TiO_2 film after solvothermal treatment (Fig. 10(d)). Rod-like $Bi_{13}S_{18}I_2$ nanocrystals were formed in the nanopores and surface of the porous TiO_2 film (Fig. 10(b, c)). The diameter of the $Bi_{13}S_{18}I_2$ nanorods in the nanopores was about 50 nm, which is slightly smaller than those on the surface, indicating that the crystal size in the nanopores is controlled by the pore size.

Fig. 9(b) shows the photocurrent-voltage (*I-V*) characteristic curves of eight solar cells under simulated AM 1.5 spectrum. The cell performance parameters of energy conversion efficiency (η), short-circuit photocurrent density (J_{sc}), open-circuit voltage (V_{oc}), and fill factor (*FF*) evaluated from the *I-V* curves were summarised in Table S2. These cells exhibited η, J_{sc}, V_{oc}, and *FF* values in the ranges of 0.53 to 0.85 %, 3.22 to 3.82 mA/cm^2, 0.51 to 0.58 V, and 29.3 to 38.3 %, respectively. The relatively high repeatability of the cell performance can be attributed to the high stability of $Bi_{13}S_{18}I_2$. The highest η value is 0.85 % with cell parameters of J_{sc}=3.82 mA/cm^2, V_{oc}=0.58 V, and *FF*=38.3 %. Although the PCE of these preliminary solar cells are still low, these results reveal the potential of $Bi_{13}S_{18}I_2$ as a light absorber for photovoltaics and photoelectric devices. The low PCE can be attributed mainly to low J_{sc} and *FF* values of the cell. Many factors, such as the cell structure, the thickness of the $Bi_{13}S_{18}I_2$ and TiO_2 films, crystallinity of the $Bi_{13}S_{18}I_2$, and hole-transporting material, can affect the J_{sc} and *FF* values. The optimization of these factors will further improve the solar cell performance. Moreover, the $Bi_{13}S_{18}I_2$ band gap of 0.75 eV is smaller than the ideal bandgap of 1.4 eV for a single p-n junction solar cell,[46] which also limits the maximum PCE value. To give the precise evaluation of the ultimate potential of $Bi_{13}S_{18}I_2$ as light absorber for the photovoltaics, the further detailed studies, such as the lifetime, photoluminescence quantum efficiency, and Urbach energy, are expected.

Journal of Materials Chemistry C Accepted Manuscript

View Article Online
DOI: 10.1039/C9TC05159B

Published on 24 January 2020. Downloaded by Goteborgs Universitet on 1/28/2020 9:01:40 AM.

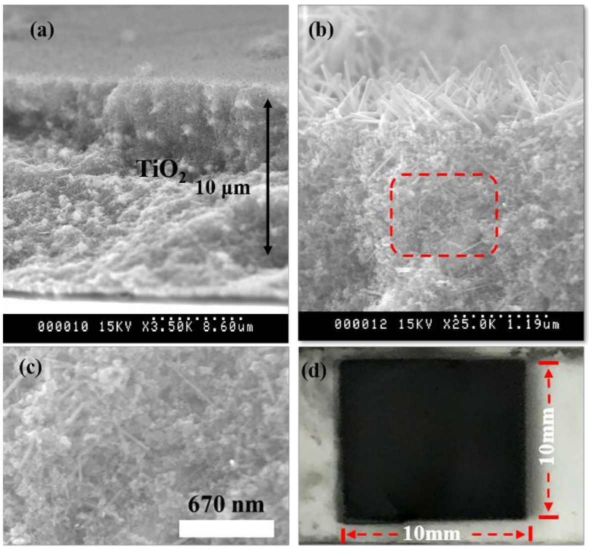

Fig. 10. (a, b) Cross-sectional FE-SEM images and (d) photograph of FTO/TiO$_2$/Bi$_{13}$S$_{18}$I$_2$ electrode. (c) is enlarge red square in (b).

Conclusions

The solvothermal process is a facile method for the synthesis of bismuth chalcogenide iodide compounds of Bi$_{13}$S$_{18}$I$_2$ and BiSI. The formations of Bi$_{13}$S$_{18}$I$_2$ and BiSI are strongly dependent on the S/Bi mole ratio, reaction temperature, and solvent. BiSI can be formed under low S/Bi mole ratio conditions, but it is unstable and easily converts to Bi$_{13}$S$_{18}$I$_2$ under higher S/Bi mole ratio conditions. Both Bi$_{13}$S$_{18}$I$_2$ and BiSI have similar rod-like crystal morphology due to their ribbon-like and chain structures. Bi$_{13}$S$_{18}$I$_2$ is an n-type semiconductor with a narrow bandgap of 0.75 eV. The strong light absorbance of Bi$_{13}$S$_{18}$I$_2$ in a wide wavelength range from UV to NIR suggests that it is a promising light absorber material for solar cells. Uniform Bi$_{13}$S$_{18}$I$_2$ nanorod film can be fabricated on the porous TiO$_2$ electrode by a modified solvothermal process. The preliminary PV study demonstrates a PCE of 0.85%, revealing the potential of the Bi$_{13}$S$_{18}$I$_2$ light absorber for a new type of solar cell that can be fabricated by low-cost solution process.

Conflicts of interest

There are no conflicts to declare.

Acknowledgements

This work was supported by The Murata Science Foundation and The Grants-in-Aid for Scientific Research (B) (No. 26289240) from Japan Society for the Promotion of Science.

Notes and references

1 L. M. Peter, *Philos Trans A Math Phys Eng Sci*, 2011, **369**, 1840-1856.
2 W. Hermann, *Energy*, 2006, **31**, 1685-1702.
3 J. Peng, L. Lu and H. Yang, *Renewable and Sustainable Energy Reviews*, 2013, **19**, 255-274.
4 M. Powalla, S. Paetel, E. Ahlswede, R. Wuerz, C. D. Wessendorf and T. Magorian Friedlmeier, *Applied Physics Reviews*, 2018, **5**, 041602.
5 H. Morrow, 2010, DOI: 10.1002/0471238961.0301041303011818.a01.pub3.
6 M. A. Green, A. Ho-Baillie and H. J. Snaith, *Nature Photonics*, 2014, **8**, 506-514.
7 M. Gratzel, *Nat Mater*, 2014, **13**, 838-842.
8 NREL Efficiency Chart. This Plot is Courtesy of the National Renewable Energy Laboratory, Golden, CO. Available online: https://www.nrel.gov/pv/assets/pdfs/best-reserch-cell-e_ciencies.20190411.pdf (accessed on 14 April 2019).
9 L. Meng, J. You and Y. Yang, *Nat Commun*, 2018, **9**, 5265.
10 Z. Xiao, W. Meng, J. Wang and Y. Yan, *ChemSusChem*, 2016, **9**, 2628-2633.
11 Y. Zhang, J. Yin, M. R. Parida, G. H. Ahmed, J. Pan, O. M. Bakr, J. L. Bredas and O. F. Mohammed, *J Phys Chem Lett*, 2017, **8**, 3173-3177.
12 P. Wang, X. Zhang, Y. Zhou, Q. Jiang, Q. Ye, Z. Chu, X. Li, X. Yang, Z. Yin and J. You, *Nat Commun*, 2018, **9**, 2225.
13 L.-M. Wu, X.-T. Wu and L. Chen, *Coordination Chemistry Reviews*, 2009, **253**, 2787-2804.
14 A. Walsh, D. J. Payne, R. G. Egdell and G. W. Watson, *Chem Soc Rev*, 2011, **40**, 4455-4463.
15 F. Giustino and H. J. Snaith, *ACS Energy Letters*, 2016, **1**, 1233-1240.
16 Y. Y. Sun, J. Shi, J. Lian, W. Gao, M. L. Agiorgousis, P. Zhang and S. Zhang, *Nanoscale*, 2016, **8**, 6284-6289.
17 F. Bai, Y. Hu, Y. Hu, T. Qiu, X. Miao and S. Zhang, *Solar Energy Materials and Solar Cells*, 2018, **184**, 15-21.
18 K. Mistewicz, M. Nowak and D. Stroz, *Nanomaterials (Basel)*, 2019, **9**.
19 C. Deng, H. Guan and X. Tian, *Materials Letters*, 2013, **108**, 17-20.
20 L. Zhu, Y. Xie, X. Zheng, X. Yin and X. Tian, *Inorganic Chemistry*, 2002, **41**, 4560-4566.
21 H. Shi, W. Ming and M.-H. Du, *Physical Review B*, 2016, **93**.
22 A. M. Ganose, K. T. Butler, A. Walsh and D. O. Scanlon, *Journal of Materials Chemistry A*, 2016, **4**, 2060-2068.
23 H. Kunioku, M. Higashi and R. Abe, *Sci Rep*, 2016, **6**, 32664.
24 N. T. Hahn, A. J. E. Rettie, S. K. Beal, R. R. Fullon and C. B. Mullins, *The Journal of Physical Chemistry C*, 2012, **116**, 24878-24886.
25 D. Tiwari, F. Cardoso-Delgado, D. Alibhai, M. Mombrú and D. J. Fermín, *ACS Applied Energy Materials*, 2019, **2**, 3878-3885.
26 W. L. Huang and Q. Zhu, *J Comput Chem*, 2009, **30**, 183-190.
27 D. Arivuoli, F. D. Gnanam and P. Ramasamy, *Journal of Materials Science*, 1986, **21**, 2835-2838.
28 W. J. Fa, P. J. Li, Y. G. Zhang, L. L. Guo, J. F. Guo and F. L. Yang, *Advanced Materials Research*, 2011, **236-238**, 1919-1922.
29 R. Groom, A. Jacobs, M. Cepeda, R. Drummey and S. E. Latturner, *Chemistry of Materials*, 2017, **29**, 3314-3323.
30 C. H. Ho, Y. H. Chen, Y. K. Kuo and C. W. Liu, *Chem Commun (Camb)*, 2017, **53**, 3741-3744.
31 G. Shen, D. Chen, K. Tang, L. Huang and Y. Qian, *Journal of Crystal Growth*, 2003, **249**, 331-334.
32 Y. Chen, G. Tian, T. Feng, W. Zhou, Z. Ren, T. Han, Y. Xiao and H. Fu, *CrystEngComm*, 2015, **17**, 6120-6126.

Journal of Materials Chemistry C Accepted Manuscript

View Article Online
DOI: 10.1039/C9TC05139B

Published on 24 January 2020. Downloaded by Goteborgs Universitet on 1/28/2020 9:01:40 AM.

Journal of Materials Chemistry C Accepted Manuscript

33 Z. Wu, Y. Jiang, X. Xiong, S. Ding, Y. Shi, X. Liu, Y. Liu, Z. Huang and J. Hu, *Catalysis Science & Technology*, 2017, **7**, 3464-3468.

34 Y. Yan, Y. Xu, S. Lei, X. Ou, L. Chen, J. Xiong, Y. Xiao and B. Cheng, *Dalton Transactions*, 2018, **47**, 3408-3416.

35 C. Chen, G. A. Sewvandi, T. Kusunose, Y. Tanaka, S. Nakanishi and Q. Feng, *CrystEngComm*, 2014, **16**, 8885.

36 C. Chen, L. Xu, G. A. Sewvandi, T. Kusunose, Y. Tanaka, S. Nakanishi and Q. Feng, *Crystal Growth & Design*, 2014, **14**, 5801-5811.

37 Y. Zhou, L. Wang, S. Chen, S. Qin, X. Liu, J. Chen, D.-J. Xue, M. Luo, Y. Cao, Y. Cheng, E. H. Sargent and J. Tang, *Nature Photonics*, 2015, **9**, 409-415.

38 A. Audzijonis, R. Žaltauskas, R. Sereika, L. Žigas and A. Rėza, *Journal of Physics and Chemistry of Solids*, 2010, **71**, 884-891.

39 G. E. Jellison and F. A. Modine, *Applied Physics Letters*, 1996, **69**, 2137-2137.

40 M.-Y. K. Sang-An Park, Ji-Yong Lim, Byong-Seo Park, Jeong-Dae Koh, and Wea-Tek Kim, 1995.

41 M. A. Butler, *Journal of Applied Physics*, 1977, **48**, 1914-1920.

42 R. C. Newman, *Reports on Progress in Physics*, 1982, **45**, 1163-1210.

43 J. Grigas, E. Talik, M. Adamiec, V. Lazauskas and V. Nelkinas, *Journal of Electron Spectroscopy and Related Phenomena*, 2006, **153**, 22-29.

44 J. You, Z. Hong, Y. M. Yang, Q. Chen, M. Cai, T. B. Song, C. C. Chen, S. Lu, Y. Liu, H. Zhou and Y. Yang, *ACS Nano*, 2014, **8**, 1674-1680.

45 A. W. Bott, *Current Separations*, 1998, 87-91.

46 W. Shockley and H. J. Queisser, *Journal of Applied Physics*, 1961, **32**, 510-519.

View Article Online
DOI: 10.1039/C9TC05139B

Published on 24 January 2020. Downloaded by Goteborgs Universitet on 1/28/2020 9:01:40 AM.

Journal of Materials Chemistry C Accepted Manuscript

TOC GRAPHICS

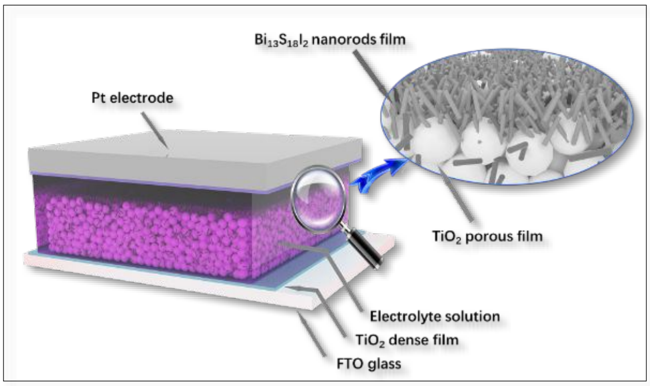

$Bi_{13}S_{18}I_2$-based solar cell